Supplementary Materials

Piperidine-Based Ionic Liquid Additive with Electrostatic Shielding and Redox Enabling Advanced Lithium-Oxygen Batteries

Meng-Lin Gao[a], Qian-Yan Wang[a], Ya-Ling Liao[a], Wei-Rong Chen[a], Zhong-Yu Huang[a], Xin-Xin Zhuang[a] and Xiao-Ping Zhang*[a,b]

a School of Electrical Engineering, Southwest Jiaotong University, Chengdu, 610031, China

b Tianfu Yongxing Laboratory

**E-mail: zxp@swjtu.edu.cn (X. Zhang)*

Experimental[1,2]

Materials preparation

Cathode preparation: Multi-walled carbon nanotubes (MWCNTs, XFNANO, length: 0.5−2 μm, diameter: 20−30 nm), single-layer graphene (XFNANO, diameter: 0.5−5 μm, thickness: 0.8−1.2 nm), and polyvinylidene fluoride (PVDF, Adamas) were weighed and mixed in a ratio of 8:1:1, and then an appropriate amount of N-Methyl-2-Pyrrolidone (NMP) was added to the mixture. The mixed slurry was then sonicated for at least 30 minutes and subsequently stirred magnetically for over 20 hours. The slurry was evenly coated onto custom-made circular carbon paper (diameter: 12 mm, thickness: ~0.2 mm) using a scraper. Then the carbon paper was dried in a vacuum drying oven at 80 °C for at least 24 hours, until the NMP was completely evaporated. The prepared MWCNT cathode was transferred to a glovebox filled with Ar gas (H_2O and O_2 concentrations < 0.01 ppm) for further use. The loading weight of the cathode was approximately 0.1 mg, with a loading area of approximately 0.25 cm^2.

Electrolyte preparation: For Li-O_2 batteries, 1M bis(trifluoromethane)sulfonimide lithium (LiTFSI) was dissolved in tetraglyme (TEGDME). 100 mM lithium bromide (LiBr, Adamas, 99.99%), 1-allyl-3-vinylimidazolium bromide (AVIB, Adamas, 99%), or 1-methyl-1-propylpiperidinium bromide (PP13Br, Adamas, 98%) are added as additives. For Li-Li symmetric batteries and Li-Cu half-batteries, the solvent was replaced by a mixed solvent of ethylene carbonate/dimethyl carbonate (EC/DMC, 1:1 v/v).

Watman GF/B and GF/C glass fiber separators were cut into discs with a diameter of 16 mm and set aside. Copper and lithium foils (0.2 mm) were cut into discs with diameters of 12 and 16 mm, respectively.

Battery preparation

Li-O_2 batteries were assembled using CR2032 coin cells containing O_2 channel. The assembly followed the order of lithium foil, GF/B glass fiber separator, and MWCNT cathode, with ~140μL of electrolyte added. The assembled batteries were placed in a specialized glass test device and filled with 1.5 m bar of high-purity O_2. The assembly of Li-Li symmetric batteries and Li-Cu half-batteries used a GF/C glass fiber separator, added ~60μL of electrolyte, and the cathodes were lithium foil and copper foil, respectively.

Electrochemical analysis

All constant-current charge/discharge tests were conducted using the LAND CT3001A electrochemical testing system. Cycling voltammetry (CV) tests were performed using the Bio-logic VSP with a voltage range of 2.0−4.2 V and a scan rate of 0.1 mV/s. Electrochemical impedance spectroscopy (EIS) analysis of Li-Li symmetric batteries was carried out using the Gamry Interface 5000 E, with a voltage amplitude of 10 mV and a frequency range from 10^6 to 10^{-1}. All tests were conducted at room temperature.

Characterization

The cycled Li-O_2 battery was disassembled in a glovebox filled with argo. The Li anode was then removed and washed with 1,2-dimethoxyethane (DME) for at least 30 minutes to ensure thorough removal of residual electrolyte from the electrode surface. Subsequently, the electrode was dried for over 2 hours before characterization. Ensuring that the sample was not exposed to air throughout the transfer from the glovebox to the analysis equipment. The surface morphology of the Li anode was observed using field emission scanning electron microscopy (SEM, Apreo 2C). X-ray photoelectron spectroscopy (XPS) was employed to investigate the surface composition of the Li anode under different electrochemical states, with the binding energy calibrated using the C 1s peak corresponding to the C−C bond at 284.8 eV. XPS measurements were conducted using the Thermo Scientific K-Alpha TM+ spectrometer with a monochromatic Al Kα X-ray source.

Calculation

All the calculations were performed according to density functional theory (DFT) by GAUSSIAN09.[3] Geometry optimizations and frequency calculations were carried out at B3LYP/6−311+G** level with D3 empirical dispersion correction.[4] No imaginary frequencies appeared after optimizations, which indicated stationary states were found. The coordinate data of Li^+-TEGDME, $PP13^+$, and LITFSI are shown in Tables S1−S3.

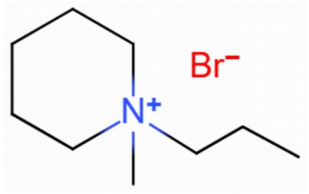

Fig. S1. Structural and Molecular Formulas of 1-Methyl-1-Propylpiperidinium Bromide ($C_9H_{20}BrN$).

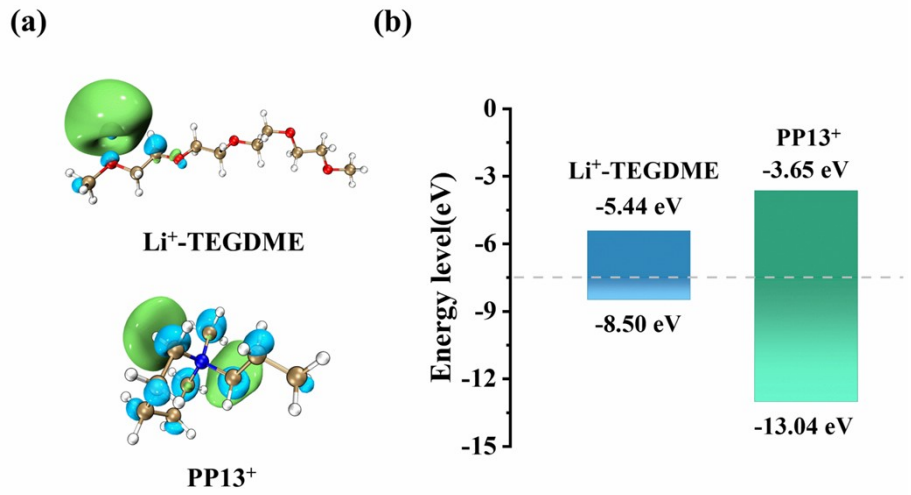

Fig. S2. (a) The visual LUMOs and (b) the LUMO and HOMO energy levels of Li^+-TEGDME and $PP13^+$.

In the electrolyte, due to the weak interactions between large-volume cations with dispersed positive charges and anions and the intrinsic positive charge of $PP13^+$ being electrostatically repelled, more anions ($TFSI^-$and Br^-) are promoted to participate in the solvation structure of Li^+. [5,6]

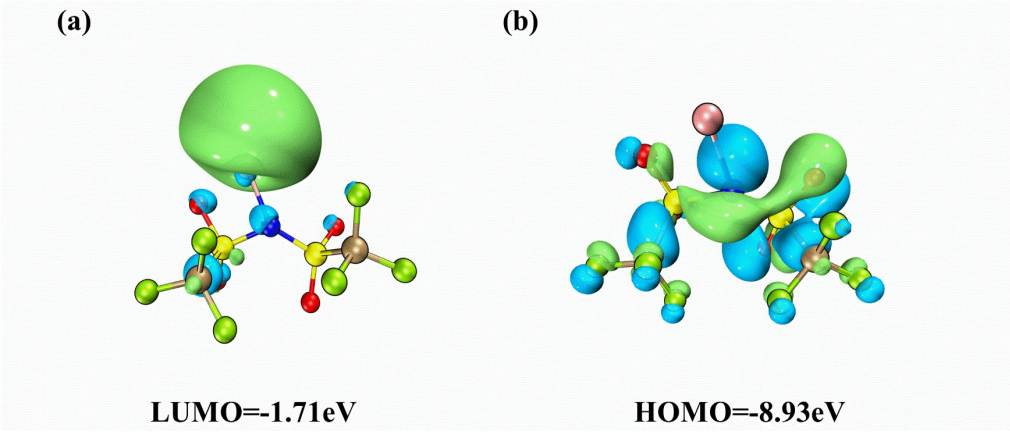

Fig. S3. Visualization (a) LUMO and (b) HOMO energy levels of LITFSI.

Table S1. Coordinates of Li^+-TEGDME.

No.	Atom	X	Y	Z
1	H	5.9085	-0.2007	1.3125
2	C	5.944	-0.0371	0.2253
3	O	6.6032	-1.1026	-0.4305
4	H	6.455	0.9196	0.0444
5	C	7.9498	-1.2644	-0.0179
6	C	4.5321	0.0224	-0.3302
7	O	3.8502	1.0697	0.3526
8	H	4.0439	-0.9487	-0.1779
9	H	4.5659	0.223	-1.4095
10	C	2.5552	1.3589	-0.1373
11	C	1.5119	0.3936	0.4211
12	O	0.2408	0.8068	-0.0764
13	C	-0.8315	0.0097	0.3718
14	C	-2.0824	0.5927	-0.2618
15	O	-3.203	-0.1839	0.1859
16	C	-4.4273	0.2333	-0.321
17	C	-5.4722	-0.7891	0.1048
18	O	-6.779	-0.1824	-0.0795
19	C	-7.8714	-1.1272	0.0485
20	H	8.3592	-2.1042	-0.5793
21	H	8.0158	-1.4842	1.0569
22	H	8.5449	-0.3656	-0.231
23	H	2.5285	1.3381	-1.2352
24	H	2.3127	2.3729	0.1883
25	H	1.5279	0.4294	1.5186
26	H	1.721	-0.6378	0.1072
27	H	-0.9213	0.0337	1.4674
28	H	-0.7115	-1.0389	0.0636
29	H	-2.005	0.5524	-1.3549
30	H	-2.2019	1.6397	0.0454
31	H	-4.4068	0.3362	-1.4172
32	H	-4.6916	1.2375	0.1046
33	H	-5.3371	-1.0504	1.1575
34	H	-5.4029	-1.692	-0.5058
35	H	-7.7928	-1.8872	-0.7314
36	H	-8.8023	-0.5739	-0.0722
37	H	-7.8438	-1.5929	1.036
38	Li	-6.8049	1.6259	-0.2084

Table S2. Coordinates of $PP13^{+}$.

No.	Atom	X	Y	Z
1	C	-2.4126	-1.0877	0.0248
2	C	-1.2702	-1.2351	1.0369
3	C	-0.6205	0.1115	1.3292
4	N	-0.0793	0.7897	0.0729
5	C	-1.2204	0.9285	-0.9397
6	C	-1.9238	-0.3903	-1.2501
7	C	0.3938	2.17	0.4373
8	C	1.0719	0.0076	-0.5659
9	C	2.2487	-0.3294	0.345
10	C	3.3422	-1.0382	-0.4668
11	H	-3.221	-0.5009	0.4759
12	H	-2.8321	-2.0651	-0.2194
13	H	-1.6424	-1.6279	1.9863
14	H	-0.524	-1.9524	0.6818
15	H	0.2046	0.0363	2.035
16	H	-1.3555	0.806	1.7425
17	H	-0.7918	1.3873	-1.8318
18	H	-1.9232	1.6357	-0.4943
19	H	-1.2707	-1.0519	-1.8253
20	H	-2.764	-0.1531	-1.9079
21	H	1.1695	2.1001	1.1956
22	H	-0.447	2.74	0.8291
23	H	0.7863	2.6577	-0.4539
24	H	1.4	0.6179	-1.41
25	H	0.6465	-0.908	-0.969
26	H	1.9252	-0.9843	1.158
27	H	2.6659	0.5728	0.7991
28	H	3.721	-0.3999	-1.2693
29	H	2.9702	-1.9634	-0.915
30	H	4.1831	-1.2966	0.1782

Table S3. Coordinates of LITFSI.

No.	Atom	X	Y	Z
1	C	-1.9592	-0.9676	-0.1387
2	S	-1.4899	0.8567	0.0737
3	F	-1.341	-1.4703	-1.199
4	F	-3.2766	-1.0593	-0.2971
5	F	-1.5967	-1.646	0.9549
6	O	-1.8397	1.5201	-1.1607
7	O	-2.1741	1.2474	1.3469
8	C	2.1184	-0.8106	0.2115
9	S	1.4157	0.8512	-0.3656
10	N	0.0525	0.8919	0.5745
11	F	2.2518	-0.8073	1.5459
12	F	3.3105	-1.0018	-0.3459
13	F	1.3011	-1.8064	-0.1351
14	O	2.3302	1.8476	0.1668
15	O	1.1449	0.7217	-1.7845
16	Li	-0.5562	1.5081	2.3168

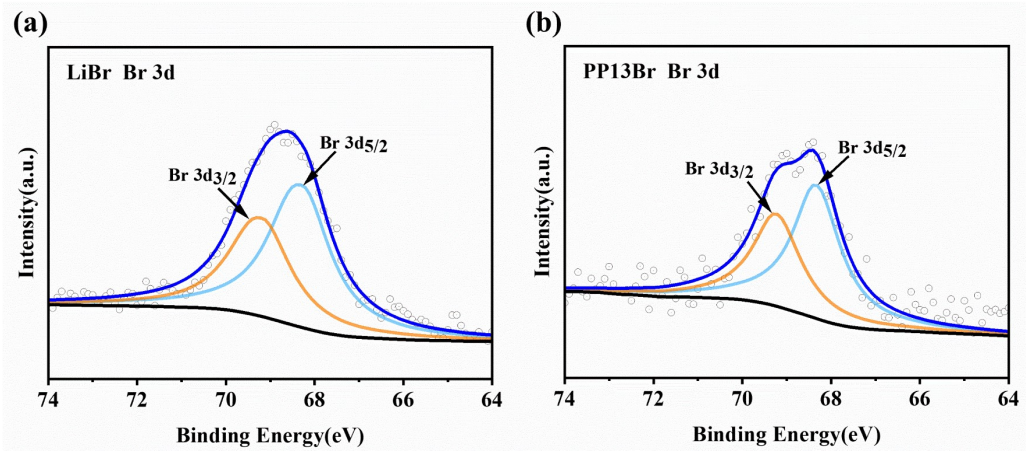

Fig. S4. Br 3d XPS spectra of Li-O_2 batteries containing (a) LiBr or (b) PP13Br after cycling.

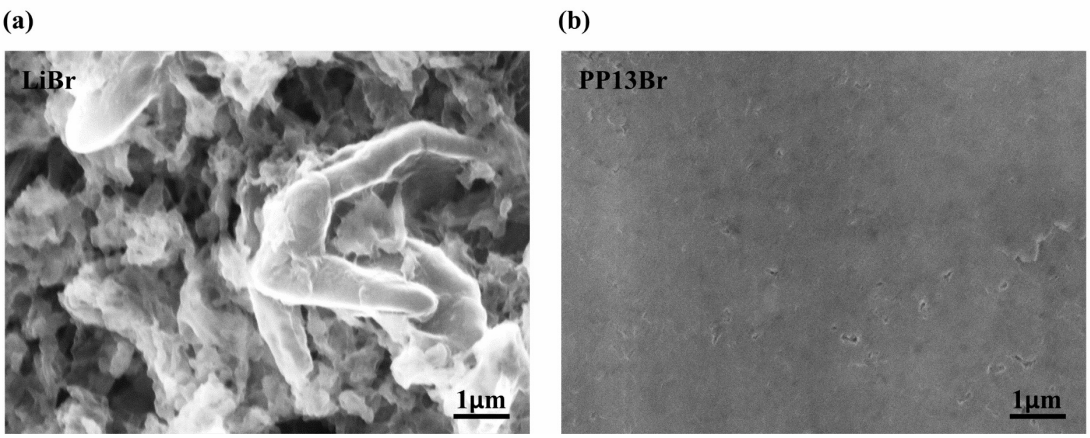

Fig. S5. The SEM images of the anode of Li-O_2 battery containing (a) LiBr or (b) PP13Br after the first cycle. The scale bar is 1 μm.

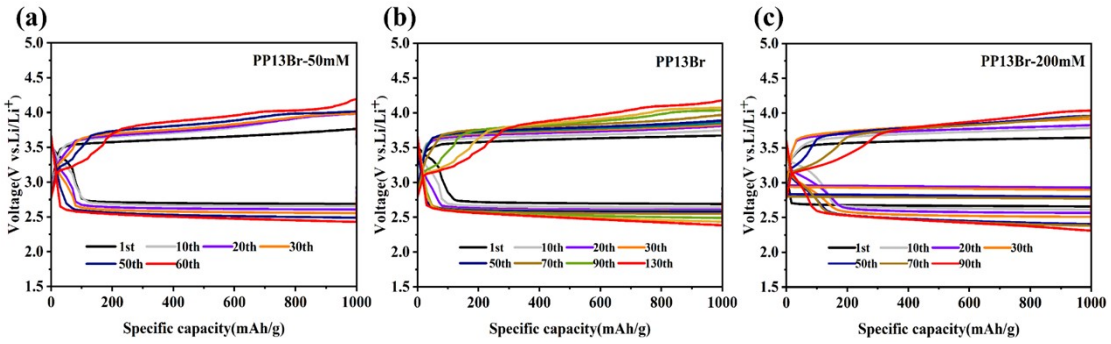

Fig. S6. The cycling responses of Li-O_2 batteries with (a) 50, (b) 100, and (c) 200 mM PP13Br-containing electrolytes at a constant current density of 1000 mA g^{-1} and a limited capacity of 1000 mAh g^{-1}.

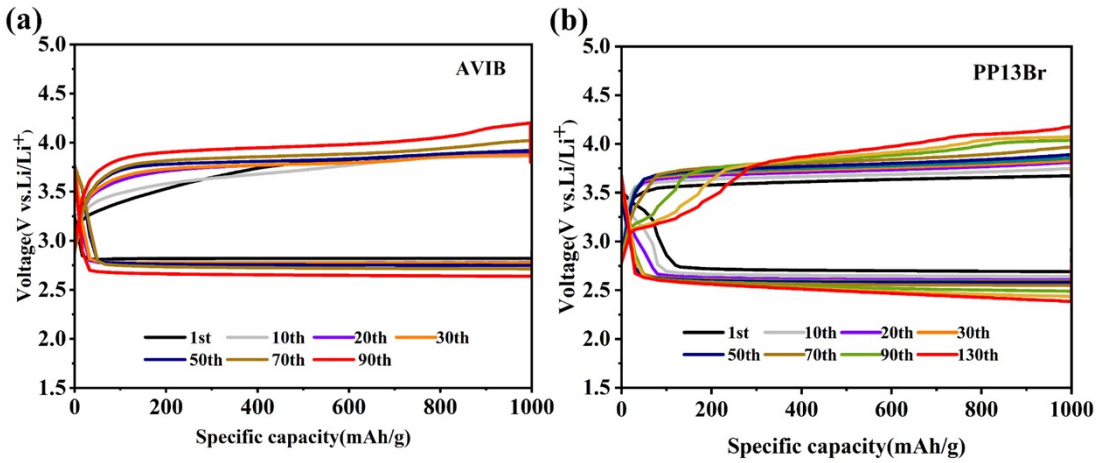

Fig. S7. Galvanostatic charge/discharge curves of Li-O_2 batteries containing (a) AVIB and (b) PP13Br.

In Li-O_2 batteries, piperidinium cations exhibit greater advantages for lowering battery overpotentials and enhancing cycling performance than imidazolium cations (1-allyl-3-vinylimidazolium bromide, AVIB), which have been widely studied for generating electrostatic shields.

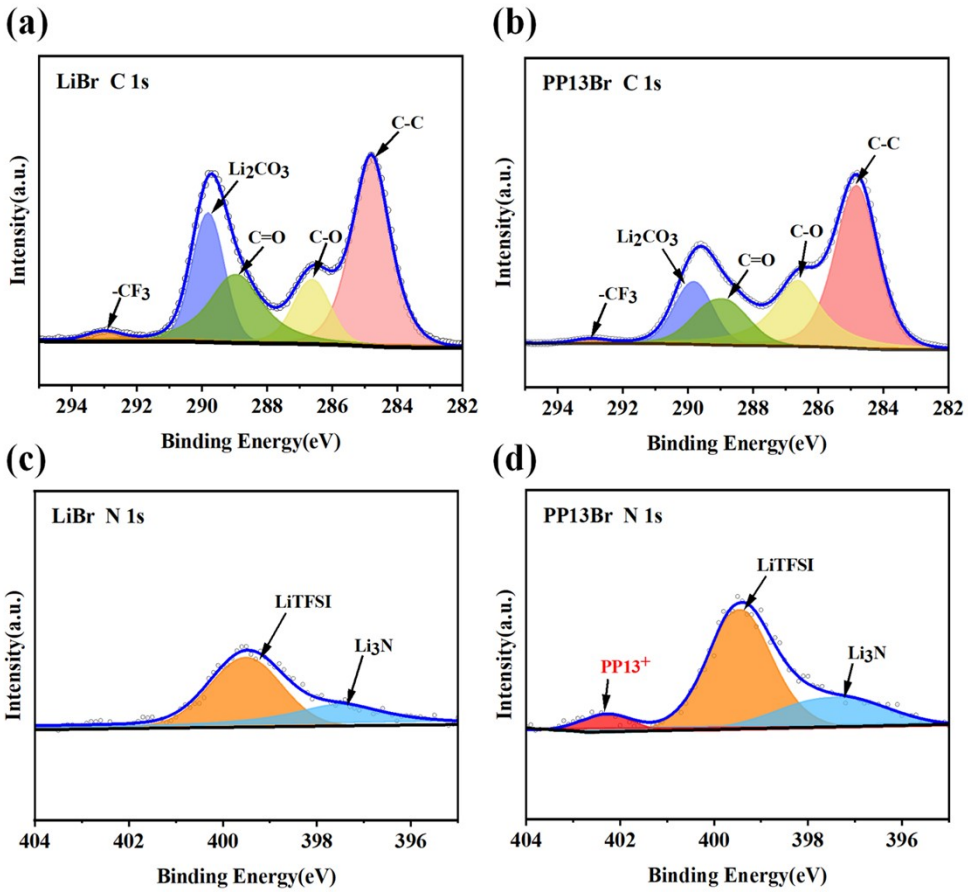

Fig. S8. XPS spectra for Li anodes in Li-O_2 batteries after 20 cycles. C 1s with (a) LiBr and (b) PP13Br. N 1s with (c) LiBr and (d) PP13Br.

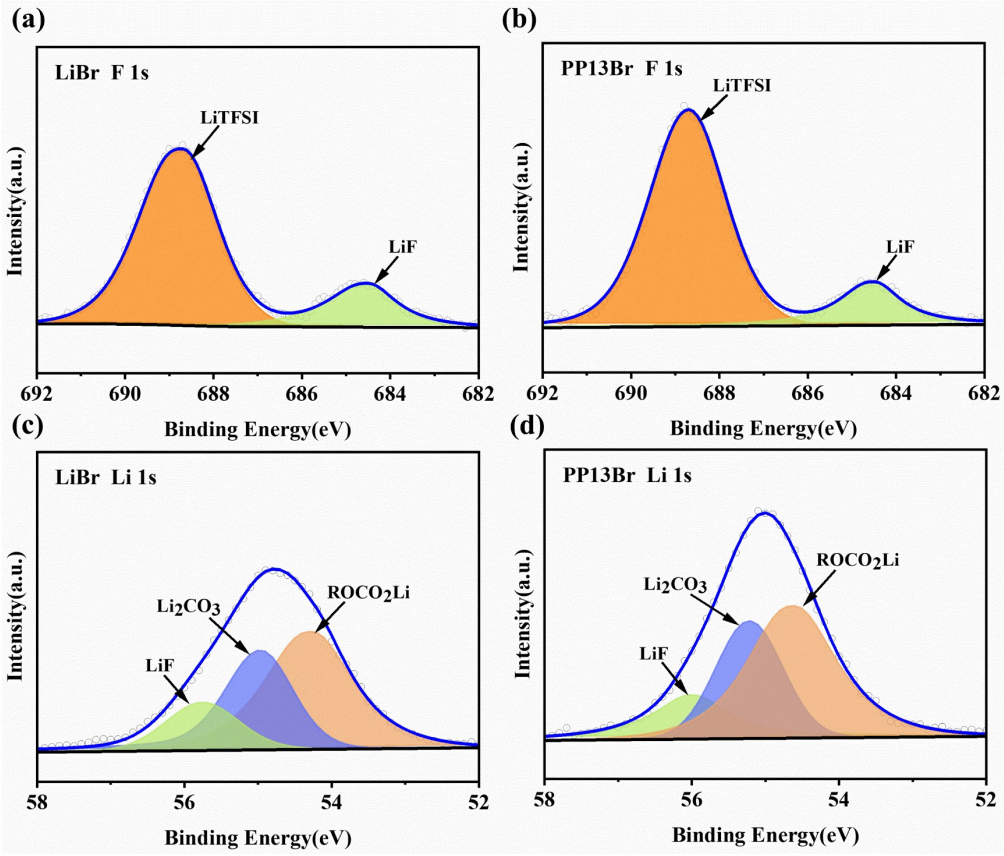

Fig. S9. XPS spectra for Li anodes in Li-O_2 batteries after 20 cycles. F 1s with (a) LiBr and (b) PP13Br. Li 1s with (c) LiBr and (d) PP13Br.

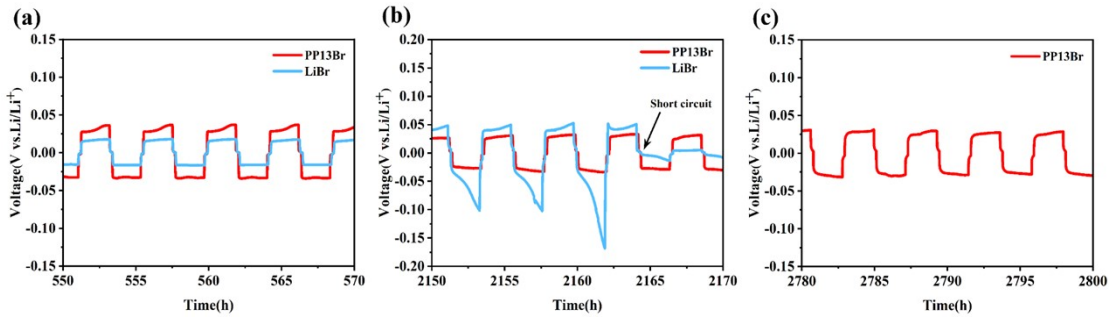

Fig. S10. Amplified charge-discharge curves of Li-Li symmetric batteries at (a) 550, (b) 2150, and (c) 2780 hours.

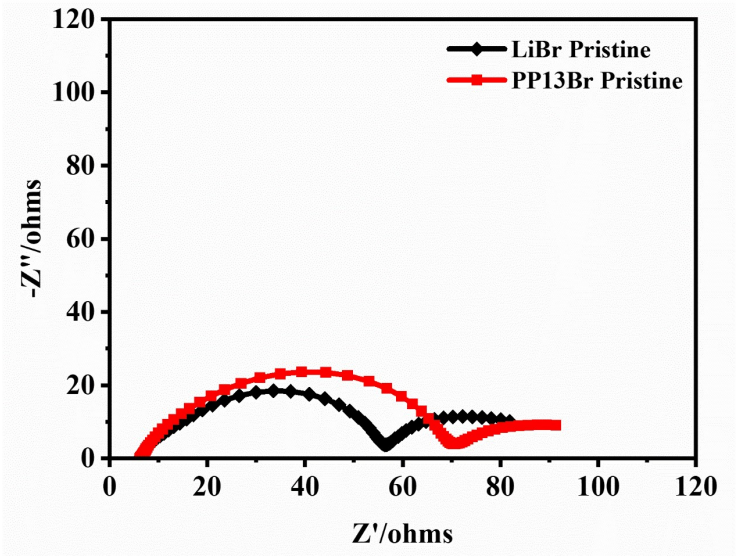

Fig. S11. EIS spectra of LiBr and PP13Br Li-Li symmetric batteries.

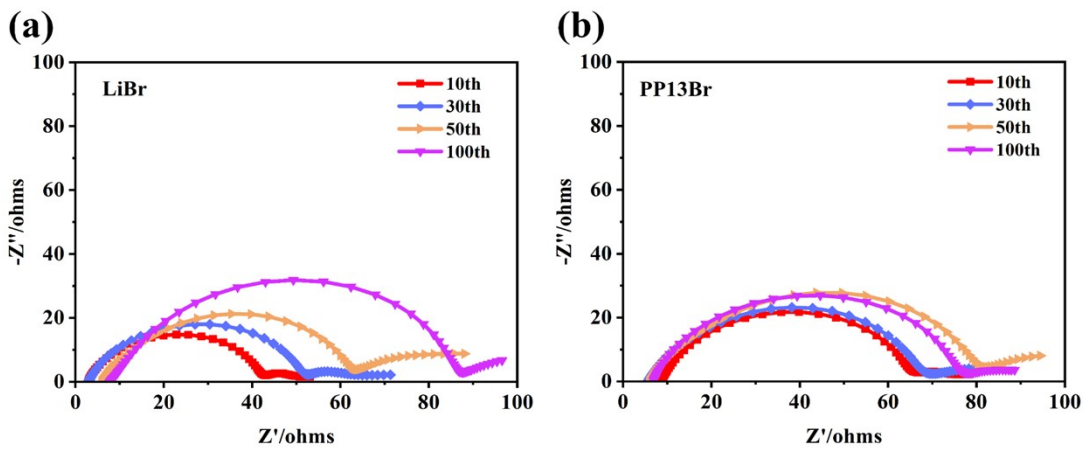

Fig. S12. EIS spectra of (a) LiBr or (b) P P13Br Li-Li symmetric batteries after different cycles.

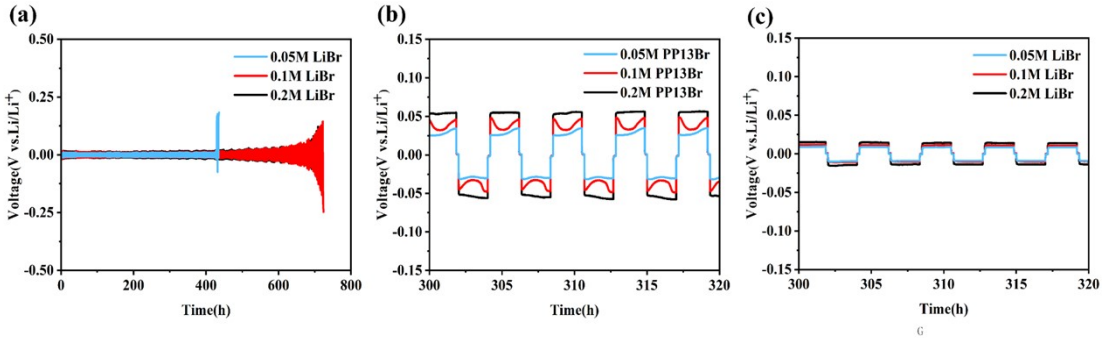

Fig. S13. (a) Li-Li symmetric batteries with different concentrations of LiBr. Amplified charge-discharge curves of Li-Li symmetric batteries with different concentrations of (b) PP13Br and (c) LiBr at 300 hours.

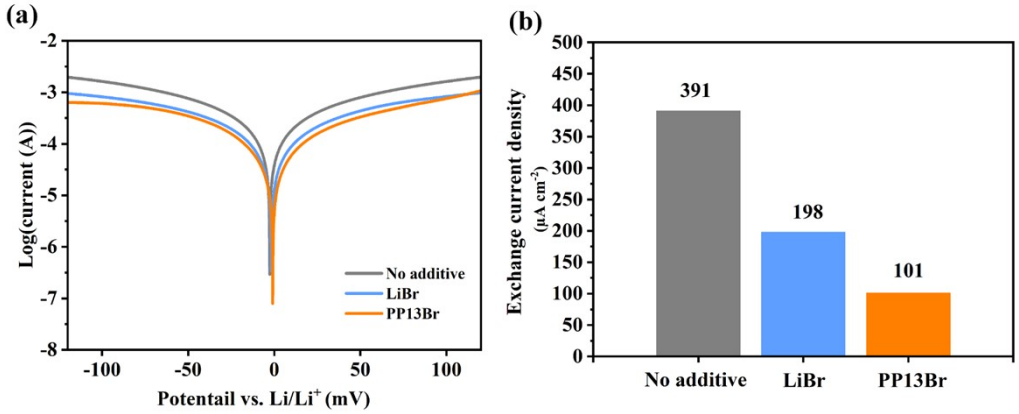

Fig. S14. (a) Tafel curves in different electrolytes. (b) Exchange current densities of different electrolytes.

For the measurement of exchange current density, CV tests were conducted on Li-Li symmetric batteries within the voltage range of -0.12 to 0.12 V at a scan rate of 1 mV/s. The exchange current density was calculated by fitting the Tafel slope of the CV scans.

In comparison, the electrolyte containing PP13Br exhibited the lowest exchange current density (101 μA cm^{-2}). This indicates that $PP13^+$ forms an electrostatic shielding layer at the protruding tips, which reduces the reaction kinetics of lithium deposition and consequently lowers the exchange current density, while also effectively protecting the protrusions from the effects of Li ions and solvents.[7-9]

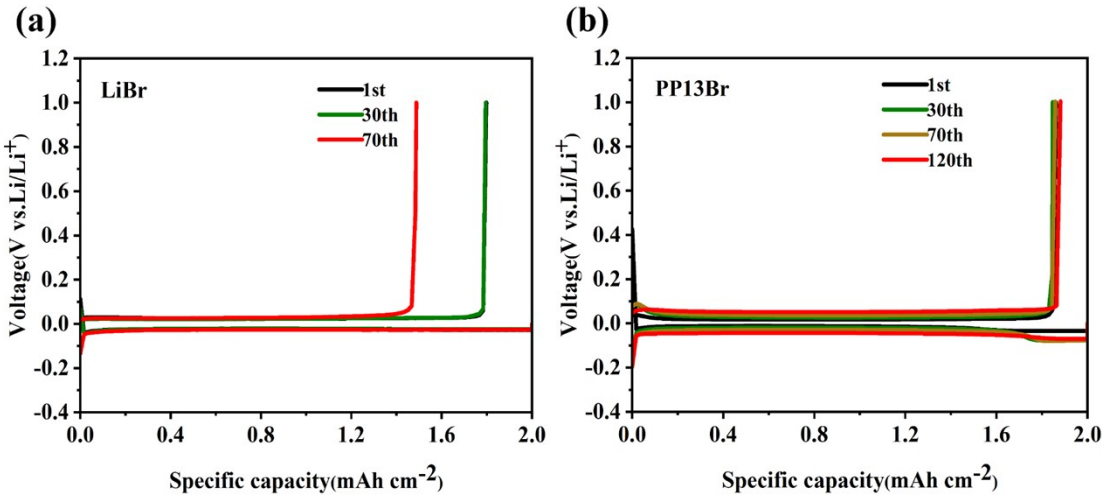

Fig. S15. Potential profiles of Li-Cu half-batteries with the addition of (a) LiBr and (b) PP13Br at specific cycles.

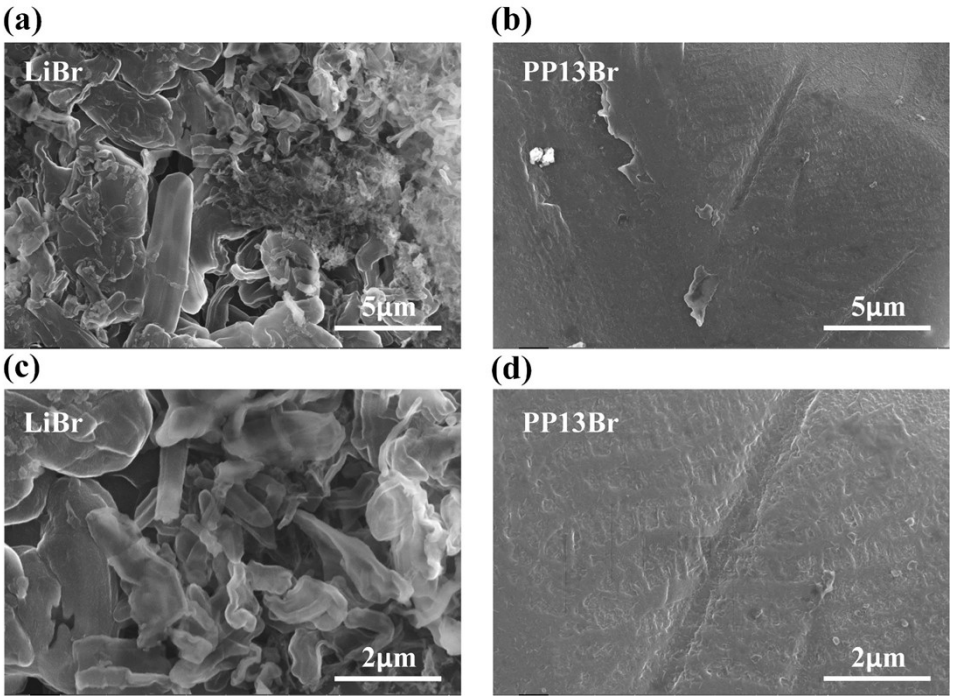

Fig. S16. SEM images of the anode in (a) LiBr-containing and (b) PP13Br-containing Li-Li symmetric batteries after 20 cycles. The scale bar is 5 μm. (c) and (d) the scale bar is 2 μm.

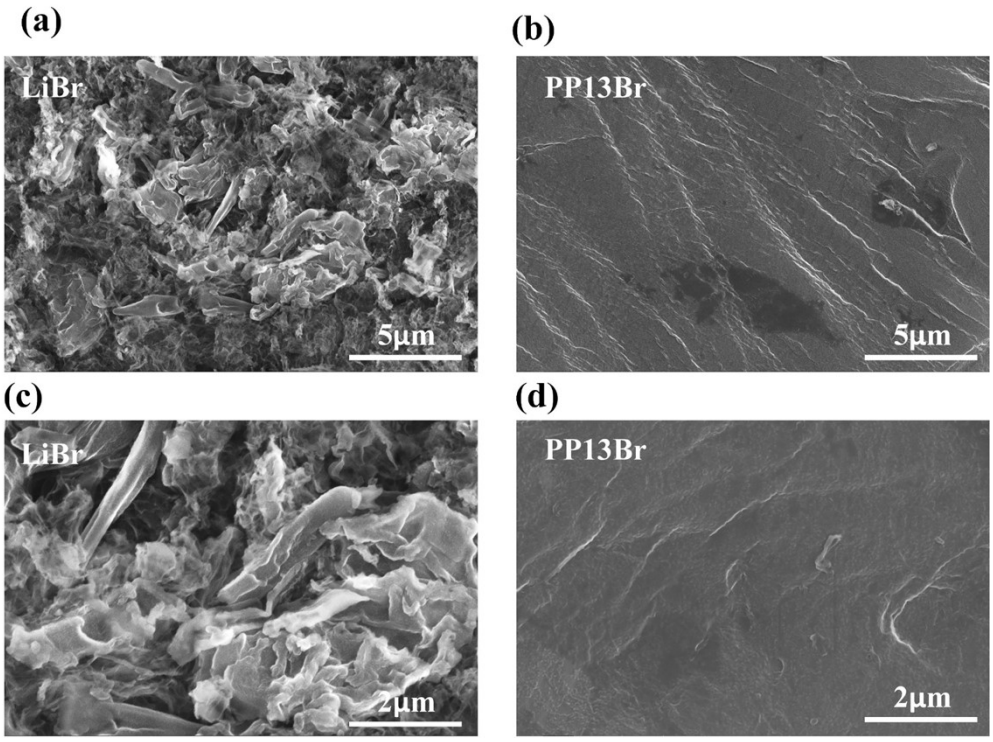

Fig. S17. SEM images of the anode in (a) LiBr-containing and (b) PP13Br-containing Li-Cu half batteries after 20 cycles. The scale bar is 5 μm. (c) and (d) the scale bar is 2 μm.

From the SEM images of the anodes of Li-Li (Fig. S16) and Li-Cu (Fig. S17) batteries after 20 cycles, it is evident that the surface of the anodes without the PP13Br additive shows significant formation of lithium dendrites. In contrast, the lithium anodes protected by electrostatic shielding exhibit relatively smooth surfaces, further demonstrating the effective inhibition of lithium dendrite growth.

References

1. C.-Y. Li, M.-S. Wu, W.-R. Chen, Q.-Y. Wang, Y.-J. Rong and X.-P. Zhang, *J. Mater. Chem. A*, 2023, **11**, 937–942.

2. Q. Wang, M. Zheng, M. Gao, Y. Liao, X. Zhang, C. Fan, W. Chen and J. Lu, *Adv Funct Materials*, 2023, 2312723.

3. M.J. Frisch, G.W. Trucks, H.B. Schlegel, G.E. Scuseria, M.A. Robb, J.R. Cheeseman, G. Scalmani, V. Barone, B. Mennucci, G.A. Petersson, H. Nakatsuji, M. Caricato, X. Li, H.P. Hratchian, A.F. Izmaylov, J. Bloino, G. Zheng, J.L. Sonnenberg, M. Hada, M. Ehara, K. Toyota, R. Fukuda, J. Hasegawa, M. Ishida, T. Nakajima, Y. Honda, O. Kitao, H. Nakai, T. Vreven, J.A. Montgomery Jr., J.E. Peralta, F. Ogliaro, M. Bearpark, J.J. Heyd, E. Brothers, K.N. Kudin, V.N. Staroverov, R. Kobayashi, J. Normand, K. Raghavachari, A. Rendell, J.C. Burant, S.S. Iyengar, J. Tomasi, M. Cossi, N. Rega, N.J. Millam, M. Klene, J.E. Knox, J.B. Cross, V. Bakken, C. Adamo, J. Jaramillo, R. Gomperts, R.E. Stratmann, O. Yazyev, A.J. Austin, R. Cammi, C. Pomelli, J.W. Ochterski, R.L. Martin, K. Morokuma, V.G. Zakrzewski, G.A. Voth, P. Salvador, J.J. Dannenberg, S. Dapprich, A.D. Daniels, O. Farkas, J.B. Foresman, J.V. Ortiz, J. Cioslowski, D.J. Fox, Gaussian 09, Revision B.01, Gaussian, Inc., Wallingford CT, 2010.

4. S. Grimme, J. Antony, S. Ehrlich and H. Krieg, *The Journal of Chemical Physics*, 2010, **132**, 154104.

5 J. Gu, Y. Jia, X. Ren, S. Li and T. Yan, Journal of Molecular Liquids, 2023, **369**, 120815.

6 Z. Wang, R. Han, H. Zhang, D. Huang, F. Zhang, D. Fu, Y. Liu, Y. Wei, H. Song, Y. Shen, J. Xu, J. Zheng, X. Wu and H. Li, Adv Funct Materials, 2023, **33**, 2215065.

7. Y. Liu, X. Xu, M. Sadd, O. O. Kapitanova, V. A. Krivchenko, J. Ban, J. Wang, X. Jiao, Z. Song, J. Song, S. Xiong and A. Matic, Advanced Science, 2021, 8, 2003301.

8. J. Jang, J. Shin, S. Ko, H. Park, W. Song, C. B. Park and J. Kang, *Advanced Energy Materials*, 2022, **12**, 2103955.

9. Z. Huang, S. Choudhury, H. Gong, Y. Cui and Z. Bao, *J. Am. Chem. Soc.*, 2020,

142, 21393–21403.